
GNUMAP: A PARAMETER-FREE APPROACH TO UNSUPERVISED DIMENSIONALITY REDUCTION VIA GRAPH NEURAL NETWORKS

Jihee You
 Data Science Institute
 University of Chicago
 Chicago, IL 60605
jiheeyou@uchicago.edu

So Won Jeong
 Booth School of Business
 University of Chicago
 Chicago, IL 60605
sowonjeong@uchicago.edu

Claire Donnat
 Department of Statistics
 University of Chicago
 Chicago, IL 60605
cdonnat@uchicago.edu

August 1, 2024

ABSTRACT

With the proliferation of Graph Neural Network (GNN) methods stemming from contrastive learning, unsupervised node representation learning for graph data is rapidly gaining traction across various fields, from biology to molecular dynamics, where it is often used as a dimensionality reduction tool. However, there remains a significant gap in understanding the quality of the low-dimensional node representations these methods produce, particularly beyond well-curated academic datasets. To address this gap, we propose here the first comprehensive benchmarking of various unsupervised node embedding techniques tailored for dimensionality reduction, encompassing a range of manifold learning tasks, along with various performance metrics. *We emphasize the sensitivity of current methods to hyperparameter choices — highlighting a fundamental issue as to their applicability in real-world settings where there is no established methodology for rigorous hyperparameter selection.* Addressing this issue, we introduce GNUMAP, a robust and parameter-free method for unsupervised node representation learning that merges the traditional UMAP approach with the expressivity of the GNN framework. We show that GNUMAP consistently outperforms existing state-of-the-art GNN embedding methods in a variety of contexts, including synthetic geometric datasets, citation networks, and real-world biomedical data — making it a simple but reliable dimensionality reduction tool.

1 Introduction

Consider the following biological problem: given a set of gene expressions at various locations within a tissue sample (for instance, a slice of mouse brain tissue), how can we aggregate information to discover spatial domains with coherent gene expression patterns? Recent methods, including [1] from which this example is adapted, have turned towards using a graph-based approach — and subsequently, Graph Neural Networks (GNNs) — to resolve this conundrum. In this setting, the data is first represented as a graph \mathcal{G} on n nodes corresponding here to the various spatial locations within the sample, each endowed with a feature vector $X_v \in \mathbb{R}^d$ (the gene expression data). Under this new formalism, Graph Neural Networks (GNNs) [2, 3] come as a natural tool for visualization and the subsequent discovery of new patterns in the data. Through the use of recursive neighborhood “convolutions”, GNNs allow indeed the creation of rich node representations that capture topological information, feature data and essential neighborhood properties, and integrate this information in a Euclidean vector representation that is amenable to any downstream machine learning task.

Unsupervised Learning on Graph Data. While the early rise in Graph Neural Network (GNN) advancements predominantly emphasized supervised learning, there has been growing interest in developing unsupervised GNN methods for learning node representations. This shift is driven by the scarcity of labeled data in numerous real-world situations, such as in the example described above, along with an increasing demand for techniques that facilitate exploratory data analysis and dimensionality reduction for graph data. However, there seems to have been a concurrent development of unsupervised learning approaches in the application community [1, 4, 5, 6, 7] and in the method community [8, 9, 10, 11, 12]. This parallel development may underscore a disconnect between the approaches devised by the methods community and the practical reality of real-world data. Specifically, the deployment of state-of-the-art

approaches evaluated on academic benchmarks appears to be impeded by two significant challenges: *(a) Ease of deployment*, and *(b) Trustworthiness of the learned representations*.

(a) Ease of deployment. From a methodological point of view, a growing number of recent approaches are leaning toward the adoption of self-supervised contrastive learning frameworks to effectively represent nodes [8, 11, 10, 9, 12]. In this setting, the trick usually consists of perturbing the input data (e.g., by masking features with probability p_f , dropping edges with probability p_e) to create two modified versions of the original data. Each of these perturbed versions of the data is then processed by a Graph Neural Network, which is trained to identify pairs of node embeddings from the two perturbed graphs that correspond to the same node in the original dataset. Examples of such training objectives include the loss proposed by [11] for their method GRACE, $\mathcal{L} = \frac{1}{2N} \left(\sum_{i=1}^N [\ell(u_i, v_i) + \ell(v_i, u_i)] \right)$,

where $\ell(u_i, v_i) = \log \left(\frac{e^{s(u_i, v_i)/\tau}}{\sum_{k=1}^N [\mathbb{1}_{\{k \neq i\}} e^{s(u_i, u_k)/\tau} + e^{s(u_i, v_k)/\tau}]} \right)$, $s : \mathbb{R}^p \times \mathbb{R}^p \rightarrow \mathbb{R}$ is the cosine similarity function, and $u_i, v_i \in \mathbb{R}^p$ are the node representation for node i stemming from the two perturbed versions of the graph. Finally, $\tau > 0$ is a temperature parameter that must be tuned. Alternatives include the loss used in CCA-SSG [8], $\mathcal{L} = \sum_{i=1}^n \|u_i - v_i\|^2 + \lambda (\|U^T U - I\|_F^2 + \|V^T V - I\|_F^2)$ where $U, V \in \mathbb{R}^{N \times p}$ are the node representation matrix of two views, $\lambda > 0$ is a hyperparameter, and $\|\cdot\|_F$ denotes the Frobenius norm. While these self-supervised learning losses have achieved state-of-the-art performance in a number of academic benchmarks, few of these methods have yet been deployed in applied settings.

One hypothesis explaining this gap is the heavy reliance of these "state-of-the-art" approaches on the correct choice of hyperparameters (for instance, λ, τ, p_f or p_e in the approaches described above). We exemplify this phenomenon through an example case in Figure 1, where we propose to deploy CCA-SSG [8] using a simple 2-layer GCN [3] to learn a 2D visualization of the nodes. We then assess the quality of the learned embeddings by learning a support vector classifier to classify the nodes, and evaluate the performance of the classification on held-out data. We note a substantial variation in embedding quality as the edge drop rate p_e , the feature mask rate p_m and the regularization parameter λ vary. This highlights the importance of selecting the "correct" set of hyperparameters: a wrong choice of hyperparameters could cause the method to significantly underperform or to learn uninformative embeddings (see Figure 1 left). However, in the unsupervised context, there is no established cross-validation technique for GNNs or

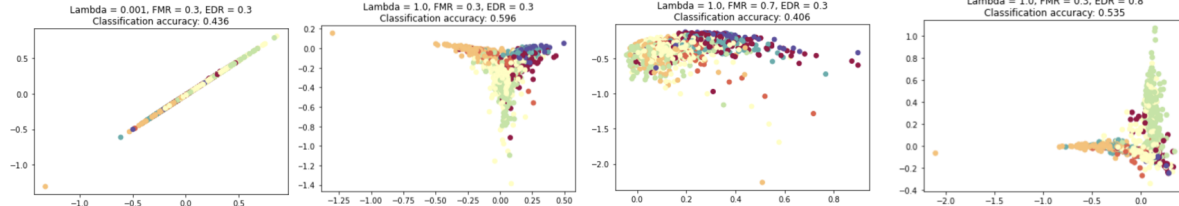


Figure 1. Node representation learning for Cora using CCA-SSG [8]. Colors represent classes. Classification accuracy was established by running a support vector machine classifier on the learned 2D node representations, using 5-fold cross-validation to fix the kernel bandwidth. We note a substantial variation in embedding quality as the parameters (regularization lambda, feature mask rate, edge drop rate) vary.

other principled technique for parameter selection at large. This significantly complicates the practical application of these methods in settings where there are no labels to evaluate the method on for hyperparameter selection.

(b) Trustworthiness. Moreover, despite the increasing adoption of graph neural networks (GNNs), there is a notable gap in research focusing on the evaluation of the quality of GNN node representations: How effectively do these embeddings capture the structural details within the data? Are they capable of accurately encoding topological information? Hypothetically, a good embedding should preserve both local and global structure in the graph while conveying a maximum amount of information. Beyond the graph setting, the need to benchmark new unsupervised approaches is underscored by the multiplication of recent publications in applied domains providing tips for performing a dimensionality reduction [13] or comparing existing tools [14, 15, 16]: with the rapidly increasing number of new methods, it becomes difficult to know which one to adopt — particularly when these methods can be quite sensitive. Many applications — particularly in biology — have a long track record of using graph-based techniques such as UMAP [17] and t-SNE [18] for dimensionality reduction. These methods have been well established, understood, and have been vetted by the myriad of applications and benchmarking tasks, including manifold learning and classification tasks, to which they have been deployed. On the other hand, while GNNs offer the potential for richer representation learning by capturing both feature and node information, these methods have not yet attained a similar level of reliability. This gap underscores *(a) the need for a comparison of GNN-based approaches to current methods*, allowing practitioners to place GNNs in the landscape of unsupervised learning methods. While GNNs offer more flexibility as they allow

combining both graph data and node covariates, this comparison is nevertheless indispensable to start evaluating them as dimensionality reduction techniques; and (b) *the need for more in-depth analysis and validation of GNNs in a variety of settings that go beyond node classification benchmarks*, and incorporate a wider variety of tasks – including learning manifolds.

Contributions. To fill this gap, we propose here a systematic comparison of learned node representations, focusing more specifically on the context of dimensionality reduction and data visualization. To bridge classical dimensionality reduction methods that do not incorporate node features with state-of-the-art GNN-based approaches, we first introduce an unsupervised learning technique inspired by UMAP [19], named GNUMAP, which integrates the UMAP framework for learning low-dimensional embeddings while being less parameter-intensive compared to contrastive learning methods. This approach facilitates a comparative analysis of self-supervised and reconstruction-based unsupervised embedding methods. We then propose to evaluate existing methods on two sets of tasks: (a) a suite of manifold learning tasks, thereby allowing us to compare GNN methods with more established benchmarks; and (b) classification tasks; Our goal is to provide practitioners with a clearer understanding of effective approaches in the unsupervised application of GNNs, thereby promoting their broader use across various applications.

2 GNUMAP: Bridging classical dimensionality reduction and Graph Neural Networks

In this section, we introduce Graph-Neural UMAP (GNUMAP), a method that allows us to bridge the Graph Neural Network (GNN) framework with established dimensionality reduction techniques proven effective on real-world data. We begin by briefly reviewing UMAP, before extending it to the analysis of graph data.

UMAP. UMAP [17], is a standard technique for dimensionality reduction of Euclidean data denoted as $\{x_i\}_{i=1}^n \in \mathbb{R}^{p_h}$, and relies partly on the graph formalism. The first step of the method consists indeed in constructing a nearest-neighbor graph based on the data points $\{x_i\}_{i=1}^n$. The connection probability between nodes in this graph is given by the formula

$$p_{ij} = p_{i|j} + p_{j|i} - p_{j|i} \times p_{i|j}, \quad (1)$$

where

$$p_{j|i} = \exp\left(-\frac{d(x_i, x_j) - \rho_i}{\sigma_i}\right). \quad (2)$$

In this context, $x_i \in \mathbb{R}^{p_h}$ denotes the original high-dimensional coordinates of input data point i , ρ_i represents the distance to the nearest neighbor of point i , and σ_i represents the local density factor around point i . UMAP finds a low-dimensional representation $y_i \in \mathbb{R}^{p_l}$, $p_l \ll p_h$ for each point x_i that minimizes the cross-entropy between connection probabilities in the high and low-dimensional space. In the low-dimensional space, UMAP uses the family of curves $f(x) = \frac{1}{1+\alpha x^{2\beta}}$ to compute the connection probability analogous to p_{ij} , which is expressed as

$$q_{ij} = \frac{1}{1 + \alpha \times d(y_i, y_j)^{2\beta}}. \quad (3)$$

By default, UMAP assumes the spread of the low-dimensional embeddings is 1 and the desired minimum distance between embeddings is 0.1. In such case, UMAP notes that $f(x) = \frac{1}{1+\alpha x^{2\beta}}$ where $\alpha = 1.57$ and $\beta = 0.89$ best models the low-dimensional connection probability. While $\alpha = 1.57$ and $\beta = 0.89$ are the default parameters, the authors of UMAP allow customizing of α and β based on the desired embedding spread and minimum distance.

The algorithm then computes the cross-entropy loss between the pairwise connection probabilities in both high (p_{ij}) and low (q_{ij}) dimensions. This cross-entropy loss is formulated as:

$$\mathcal{L} = - \sum_i \sum_j [p_{ij} \log(q_{ij}) + (1 - p_{ij}) \log(1 - q_{ij})]$$

This approach enables UMAP to find a low-dimensional representation while preserving the intrinsic topological structure of the data.

GNUMAP. By contrast, in our proposed adaptation of UMAP to the graph setting, the input of the algorithm is already a graph with either binary or weighted edges. We will denote this given input graph as $\mathcal{G} = (\mathcal{V}, \mathcal{E}, X)$, where $\mathcal{V} \in \mathbb{R}^n$ is a set of n nodes, \mathcal{E} is a set of edges along with their connection probability, and $X \in \mathbb{R}^{n \times p_h}$ be the p_h -dimensional node feature matrix. This inherent graph structure of the input allows us to bypass the initial step of traditional UMAP, which converts data into a graph with connection probability defined as in Equation 1. Similar to UMAP, our approach focuses

on achieving dimensionality reduction by identifying a low-dimensional representation that preserves the topology of the original graph.

(a) *High Dimensional Node Connectivity.* Let $\mathbf{A} \in \mathbb{R}^{n \times n}$ be the input graph's (possibly weighted) adjacency matrix. We replace the connection probability p_{ij} in Equation 2 by A_{ij} , the *observed* (and potentially weighted) connection between node i and j . This alleviates in particular any ambiguity on the choice of the parameters ρ_i and σ_i in the original method. Note here that compared to the original UMAP algorithm, if the adjacency matrix is binary, the p_{ij} 's take values in $\{0, 1\}$.

(b) *Low Dimensional Node Connectivity.* Let y_i denote the GNN embedding of datapoint i ($y_i = \text{GNN}(x_i, \mathcal{N}(i))$), where $\mathcal{N}(i)$ denote the neighborhood of point i . We further feed the GNN outputs into a differentiable batch normalization layer that scales and decorrelates the input features to reduce internal covariate shift. The effect of the DBN layer is demonstrated in Table 4 and Figure 6 in the Appendix.

Then,

$$q_{ij} = \frac{1}{1 + \alpha \times d(y_i, y_j)^{2\beta}}$$

denotes the weight of the low-dimensional node connections between y_i and y_j . This way of defining the low-dimensional connection strength q_{ij} draws significant inspiration from UMAP. As our DBN objective ensures the embedding distances are normalized, the default UMAP minimum distance of 0.1 allows interpretability in our setting, and therefore we incorporated UMAP's default constants $\alpha = 1.57$ and $\beta = 0.89$. These values allow indeed smaller tails (so more spread-out embeddings) than a baseline choice of $\alpha = \beta = 1$ (see Figure 5 in the Appendix). For a demonstration of GNUMAP performance with varying α and β , see Table 3 in the Appendix.

(c) *Loss Calculation.* GNUMAP employs a cross-entropy loss between high and low dimensional node connectivity, so the loss becomes

$$\mathcal{L} = - \sum_i \sum_j [p_{ij} \log(q_{ij}) + (1 - p_{ij}) \log(1 - q_{ij})] \quad (4)$$

For scalability purposes, GNUMAP downsamples the loss corresponding to absent edges, and samples as many negatives as positives to compute the loss. The procedure is summarized in Algorithm 1.

Algorithm 1 GNUMAP Algorithm for Output Dimension p_l

- 1: **Inputs:** Adjacency matrix $\mathbf{A} \in \mathbb{R}^{n \times n}$
- 2: $n_{\text{pos}} = \text{count}(p_{ij} > 0 \text{ in } \mathbf{P})$
- 3: $E_{\text{pos}} = \{(i, j) \in \mathcal{V} \times \mathcal{V} : p_{ij} > 0\}$
- 4: **for** epochs = 1 to 400 **do**
- 5: Sample n_{neg} negative edges, where $n_{\text{neg}} = n_{\text{pos}}$
- 6: Compute node embeddings through a graph convolution network: $\mathcal{Y}_{\text{GCN}}^{n \times p_l} = \text{GCN}(\text{Features, Edge Index})$
- 7: Apply differentiable batch normalization: $\mathcal{Y}_{\text{DBN}}^{n \times p_l} = \text{DBN}(\mathcal{Y}_{\text{GCN}})$
- 8: Compute $d(y_i, y_j)$ across all $(i, j) \in E_{\text{neg}} \cup E_{\text{pos}}$, then append to create D
- 9: Compute the corresponding low-dimensional connection probability: $Q = \frac{1}{1 + \alpha D^{2\beta}} \in \mathbb{R}^{1 \times (n_{\text{neg}} + n_{\text{pos}})}$
- 10: Access \mathbf{A} at positive edge indices and negative sampled indices to get high-dimensional connection probability
- 11: $P \in \mathbb{R}^{1 \times (n_{\text{neg}} + n_{\text{pos}})}$
- 12: Compute $\mathcal{L} = \text{Cross-Entropy}(P, Q)$ and Backpropagate \mathcal{L}
- 13: **end for**

Remark 1. GNUMAP is an auto-encoder. Using the reconstruction objective in Equation 4, it is is obvious that GNUMAP is simply an auto-encoder [20]. Auto-encoders are a class of reconstruction-based techniques that aim to find a low-dimensional representation of the data such that the distance or similarity between learned node embeddings is predictive of the existence of an edge between nodes in the original graph. The best known version of this type of approach, GAE, along with its variational version, VGAE, were first suggested in [21]. However, our proposed adaptation of UMAP differs slightly from these methods in several aspects: (i) the probability q_{ij} is defined differently. Indeed, in GAE, q_{ij} is a function of the inner product between node representations:

$$q_{ij}^{\text{GAE}} = (1 + e^{-X_i^T X_j})^{-1} = (1 + e^{\frac{d(X_i, X_j)^2 - \|X_i\|^2 - \|X_j\|^2}{2}})^{-1}.$$

Edge probabilities therefore depend both of the distance $d(X_i, X_j)$ and on the norms $\|X_i\|_2$ and $\|X_j\|_2$ of the embeddings themselves. Consequently, embeddings close to the origin will typically exhibit a higher number of

connections than embeddings farther from the origin. This allows the model to potentially build in degree heterogeneity, and places all high degree nodes towards the origin. However, in our proposed construction, this probability is solely a function of the distance. This can be beneficial, particularly when we expect the graph to have several cores, whose center (high degree nodes) should be placed far from one another. We will come back to this point in our synthetic experiments in section 3. (ii) GNUMAP uses a whitening step that allows to regularize the objective function. GNUMAP’s differentiable batch normalization design closely follows that of CLGR [12] since the effectiveness of batch whitening was already demonstrated in the previous work.

Remark 2. Contrary to self-supervised techniques for node embeddings, this proposed method does not rely on the choice of specific hyperparameters to perform well.

Remark 3. The driving hypothesis that GNUMAP leverages is that connected nodes should be close. GNUMAP is therefore amenable to homophilic networks (where adjacent nodes are presumed to be similar), rather than heterophilic networks — a limitation of our framework compared to self-supervised learning techniques.

Remark 4. Another method related to this direct extension of UMAP is SpaGCN [1]. Developed for transcriptomics applications, SpaGCN is a GCN algorithm that incorporates histological data to identify spatial domains and the associated gene expressions. From the method perspective, while SpaGCN is also an adaptation of UMAP to the graph setting, it differs from our approach in two significant ways: (i) SpaGCN directly targets creating a pre-specified number of clusters in the embedding space. The associated clusters are selected by minimizing the KL divergence between their distance in low-dimensional space, and their distance in high-dimensional space. The definitions of q and p are also quite different: SpaGCN’s q is assigned to a lower value when the embeddings are further from the cluster centers, and p is updated as the twice-normalized square of q at every three epochs. GNUMAP, by contrast, is amenable to learning a wider variety of manifolds, as it does not explicitly target the clustering of embeddings, but simply seeks to reconstruct a low-dimensional representation of the nodes that aligns with the original graph.

Overall, GNUMAP is a simple auto-encoder structure that leverages the success of UMAP in the Euclidean setting to perform dimensionality reduction. While this method is not conceptually novel (it is just an autoencoder), as we will show in our experiments section, the choice of the loss, as well as the addition of a whitening step are key to its success. This simple approach can perform well on a variety of tasks, and, as previously argued, is more interpretable and closer to many practitioners’ requirements in dimensionality reduction.

3 Evaluating GNNs’ manifold learning abilities

Having established a natural extension of UMAP to the GNN setting, we propose to benchmark these approaches on a set of toy examples evaluating their ability to correctly learn an underlying manifold structure. While this is a standard test for any dimensionality reduction technique, GNNs have not yet been evaluated in this specific context.

We first evaluate GNUMAP performance on four synthetic geometric graph datasets considered as benchmarks in the realm of unsupervised dimensionality reduction methods: the Blobs, Swissroll, Moons, and Circles datasets (see Figure 2). The datasets were generated with ground-truth low-dimensional coordinates and cluster labels, which allows us to calculate our proposed metrics and also to inspect if our metrics are coherent with the embedding visualization. The four datasets were generated with 500 nodes, each connected to its 20 nearest neighbors. For simplicity, the experiments in this work have assigned a value of 1 to positive edges and 0 to negative edges. However, the GNUMAP algorithm is applicable to any input graph preprocessed such that weaker edges are mapped closer to 0 and stronger edges closer to 1. The features were instantiated as the embeddings of a 10-component Laplacian eigenmap decomposition of the induced 20-nearest graph. The latter is indeed an established procedure to instantiate features on a graph [1]. We compare GNUMAP with state-of-the-art GNN embedding methods tailored for dimensionality reduction: DGI [9], BGRL [10], CCA-SSG [22], GAE [21], VGAE [21] and SpaGCN [1]. We also compare with well-established dimensionality reduction methods PCA, t-SNE [18], Isomap [23], Laplacian Eigenmap [24], UMAP [17], and DenseMAP [25]. Note all methods mentioned above are Euclidean methods, which enable a consistent assessment with respect to our proposed metrics. To evaluate embedding quality, we introduce metrics including but not limited to: agreement in local geometry, Spearman correlation, and classification accuracy. We refer the reader to Appendix A for a more detailed description of these metrics.

We implement a standard 2-layer GCN architecture for all GNN-based methods. Note that SpaGCN, CCA-SSG, GRACE, and BGRL are hyperparameter-heavy methods. SpaGCN requires the louvain resolution and number of neighbours for cluster initialization, as well as the penalty coefficient for embedding distance from cluster centers. Similarly, GRACE, BGRL and CCA-SSG require the specification of the regularization λ , an edge drop rate, as well as a feature mask rate. Autoencoder methods such as GNUMAP and GAE, on the other hand, are completely parameter free.

Since it is unclear which set of hyperparameters would be optimal for each dataset when deploying contrastive-learning techniques, we ran a full search for all possible hyperparameter combinations. *Note that this provides the most favorable comparison of these methods to GNUMAP, but deviates from the original unsupervised learning setting, since we are choosing the hyperparameters of the methods based on the labels — therefore making the methods more supervised. In real-world experiments, however, we would not benefit from such supervision. Despite this selection procedure, as we will show, GNUMAP still manages to outperform most methods.*

We visualize some of the embedding from the best hyperparameter combination in Figure 2. In addition to GNUMAP, we visualized GAE for comparisons with explicitly learned distance between low-dimensional embeddings, CCA-SSG and GRACE for comparisons with contrastive learning methods. We also show results from related method SpaGCN. For a complete illustration including DGI, BGRL, VGAE, as well as PCA, t-SNE, Isomap, Laplacian Eigenmap, UMAP, and DenseMAP, see Figure 7 in the appendix. Note the dimensionality reduction methods were not fitted on spectral features like the GNN-based models.

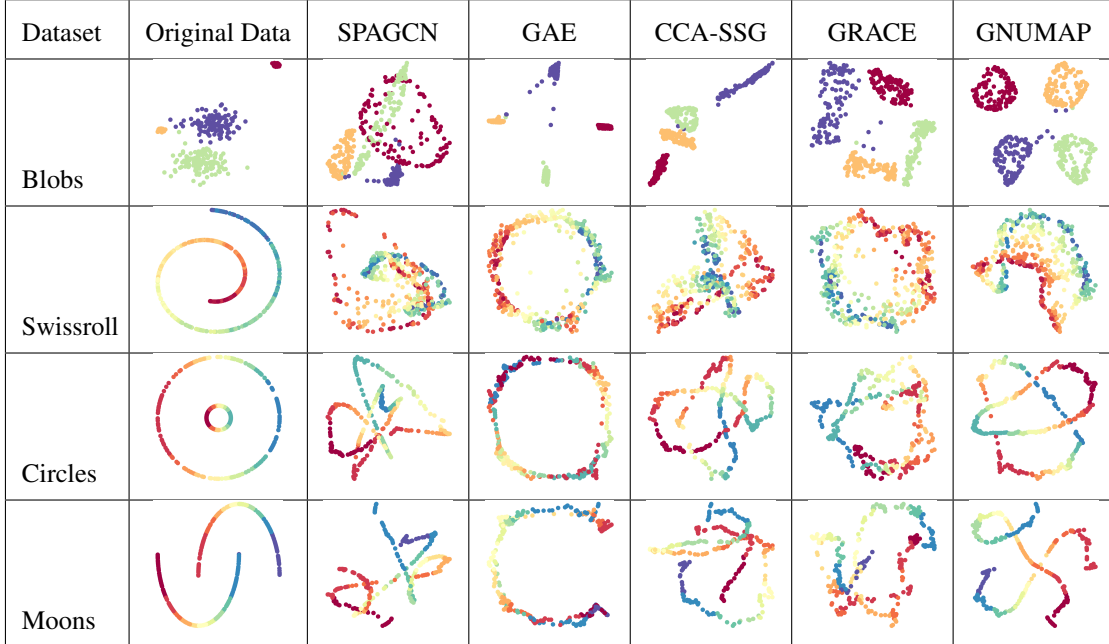


Figure 2. Node representation learning for 4 synthetic datasets : Blobs, Swissroll, Circles and Moons. Each image represents a different method of visualization.

Furthermore, we compute proposed metrics over 100 experiments and summarize the results in Table 1.

Discussion. Overall, GNUMAP consistently outperforms other self-supervised GNN-based methods in these small examples. GNUMAP successfully embeds blobs, swissroll, circles, and moons in 2-dimensions in a way that differentiates ground truth labels more clearly than state-of-the-art GNN-based methods. In Table 1, our method outperforms state-of-the-art GNN-based methods in all five of our proposed metrics and the GNUMAP embedding visualization in Figure 2 is coherent with the metrics. Note that GNUMAP successfully unrolls the Swissroll to closely resemble the original data, which is a standard synthetic dataset where linear methods fail to correctly embed.

4 Evaluating unsupervised GNNs’ embedding performance on real-world data

To assess GNUMAP’s performance across real-world data, we conducted a comparative analysis using well-established graph benchmark datasets: Cora, Citeseer, and Pubmed. They are standard citation network benchmark datasets [26]. In these networks, nodes represent scientific publications, and edges denote citation links between publications. Node features are the bag-of-words representation of papers, and node label is the academic topic of a paper.

We also incorporated the Mouse Spleen cell data [27] to assess GNUMAP performance in biological applications. The dataset was originally generated by “co-detection by indexing”(CODEX) techniques, which is to take the image of a tissue section, and at each of the tissue locations, the relevant biomarkers information is measured and recorded [27]. For our experiments, we created a 5-nearest-neighboring-cell graph from the CODEX data. While the 3-topic cluster labels in the Mouse Spleen dataset are generated by the spatial LDA model, previous work [28] has established that

Table 1. Evaluated mean and standard deviation of proposed metrics for synthetic datasets blobs, circles, moons, and swissroll over 100 experiments with GNN-based methods. The upward arrows next to metric name denote a better performance with higher metrics, whereas the downward arrows denote better performance with lower metrics. The best result is bolded, and the next best result is underlined.

Dataset	Model	Classification Accuracy \uparrow	Calinski Harabasz Score \uparrow	Davies Bouldin Score \downarrow	Spearman Correlation w/ Original Graph \uparrow	Overlap % of 50 Neighbours \uparrow
Blobs	DGI	0.65 ± 0.06	95.17 ± 90.13	5.53 ± 4.73	0.22 ± 0.09	0.52 ± 0.06
	BGRL	0.70 ± 0.07	79.26 ± 57.93	5.28 ± 7.56	0.23 ± 0.09	0.59 ± 0.05
	CCA-SSG	0.90 ± 0.08	1139.31 ± 1258.86	1.91 ± 3.87	0.52 ± 0.18	0.76 ± 0.06
	SPAGCN	0.74 ± 0.07	61.07 ± 37.80	5.89 ± 7.41	0.22 ± 0.08	0.70 ± 0.04
	GAE	0.93 ± 0.10	10456.43 ± 12149.96	<u>1.14 ± 2.25</u>	<u>0.61 ± 0.13</u>	0.58 ± 0.07
	VGAE	0.91 ± 0.10	<u>5523.10 ± 6633.58</u>	1.33 ± 2.12	<u>0.61 ± 0.13</u>	0.55 ± 0.09
	GRACE	0.84 ± 0.12	561.59 ± 631.46	2.59 ± 3.32	0.48 ± 0.18	0.73 ± 0.06
	GNUMAP	0.99 ± 0.02	1086.79 ± 173.32	0.58 ± 0.11	0.69 ± 0.10	0.97 ± 0.01
Circles	DGI	0.47 ± 0.06	34.19 ± 25.52	12.37 ± 7.42	0.23 ± 0.10	0.72 ± 0.06
	BGRL	0.49 ± 0.05	29.51 ± 16.63	10.90 ± 6.39	0.20 ± 0.07	0.76 ± 0.05
	CCA-SSG	0.53 ± 0.06	72.81 ± 92.22	10.69 ± 6.74	<u>0.40 ± 0.21</u>	<u>0.88 ± 0.04</u>
	SPAGCN	0.54 ± 0.05	31.00 ± 17.62	11.60 ± 8.73	0.21 ± 0.06	0.87 ± 0.03
	GAE	0.42 ± 0.05	40.56 ± 40.21	13.56 ± 15.43	0.38 ± 0.16	0.88 ± 0.07
	VGAE	0.42 ± 0.05	39.22 ± 21.40	11.52 ± 5.89	0.39 ± 0.16	0.83 ± 0.07
	GRACE	0.49 ± 0.05	<u>54.22 ± 60.21</u>	10.94 ± 8.63	0.36 ± 0.22	0.84 ± 0.04
	GNUMAP	0.66 ± 0.03	46.68 ± 30.84	10.88 ± 7.70	0.48 ± 0.15	0.99 ± 0.01
Moons	DGI	0.57 ± 0.06	104.58 ± 51.66	3.80 ± 2.12	0.21 ± 0.10	0.71 ± 0.06
	BGRL	0.62 ± 0.05	125.24 ± 50.80	3.08 ± 2.02	0.20 ± 0.07	0.76 ± 0.05
	CCA-SSG	0.70 ± 0.07	308.89 ± 178.11	<u>2.02 ± 1.05</u>	0.34 ± 0.18	<u>0.90 ± 0.04</u>
	SPAGCN	<u>0.70 ± 0.05</u>	160.19 ± 73.17	2.32 ± 1.42	0.21 ± 0.06	0.89 ± 0.03
	GAE	0.57 ± 0.07	768.68 ± 516.56	3.01 ± 1.70	0.33 ± 0.13	0.85 ± 0.05
	VGAE	0.56 ± 0.06	<u>620.11 ± 426.56</u>	3.36 ± 1.78	<u>0.36 ± 0.17</u>	0.80 ± 0.06
	GRACE	0.65 ± 0.06	238.53 ± 132.55	2.51 ± 1.60	0.31 ± 0.19	0.86 ± 0.04
	GNUMAP	0.88 ± 0.02	559.49 ± 163.03	0.91 ± 0.45	0.45 ± 0.13	0.99 ± 0.01
Swissroll	DGI	0.18 ± 0.03	53.80 ± 17.87	6.59 ± 1.42	0.20 ± 0.11	0.56 ± 0.06
	BGRL	0.20 ± 0.03	53.69 ± 11.91	5.95 ± 1.48	0.25 ± 0.10	0.61 ± 0.05
	CCA-SSG	0.21 ± 0.03	120.78 ± 43.25	<u>4.55 ± 1.26</u>	0.38 ± 0.16	<u>0.76 ± 0.06</u>
	SPAGCN	<u>0.22 ± 0.03</u>	93.13 ± 18.85	4.91 ± 2.55	0.27 ± 0.08	0.72 ± 0.04
	GAE	0.16 ± 0.02	<u>216.94 ± 72.76</u>	<u>5.74 ± 1.99</u>	<u>0.66 ± 0.12</u>	0.74 ± 0.03
	VGAE	0.15 ± 0.02	173.35 ± 42.33	6.41 ± 2.22	0.64 ± 0.12	0.72 ± 0.03
	GRACE	0.20 ± 0.02	102.91 ± 26.44	4.82 ± 1.32	0.37 ± 0.14	0.70 ± 0.04
	GNUMAP	0.28 ± 0.03	314.90 ± 86.80	2.53 ± 0.50	0.88 ± 0.08	0.96 ± 0.02

such topic annotations are biologically consistent with immunologist-labeled topics. Therefore, we will regard the 3-topic cluster labels as ground truth labels in the Mouse Spleen dataset for the subsequent analysis. For all experiments with real-world datasets, GNUMAP was compared against CCA-SSG, SPAGCN, and GAE.

All datasets come with or were assigned class labels, enabling a comparison between embedding visualization and our calculated metrics. For scalable metric evaluation, we randomly sampled 1000 datapoints and calculated the following metrics: classification accuracy, Calinski Harabasz score, and Davies Bouldin score. These metrics convey the general degree of embedding informativity and the quality of clustering, which is appropriate for evaluating Cora, Citeseer, Pubmed, and Mouse Spleen data as one expects some clustering among the same classes. The results are presented in Figure 3 and Table 2.

Discussion. On homophilic citation networks, GNUMAP is consistently the best or second-best for two of the three metrics: classification accuracy and Davies Bouldin score. For Cora, GNUMAP outperforms all other models in classification accuracy and Davies Bouldin score, and GNUMAP produces the second best Clinski Harabasz score after CCA-SSG. On Pubmed, GAE was the best-performing model on all three metrics, and GNUMAP was a close second. The autoencoder framework appears especially effective in this data set. GAE was the best-performing model on all three metrics for Citeseer, and GNUMAP was a close second. Autoencoder framework appears especially effective on

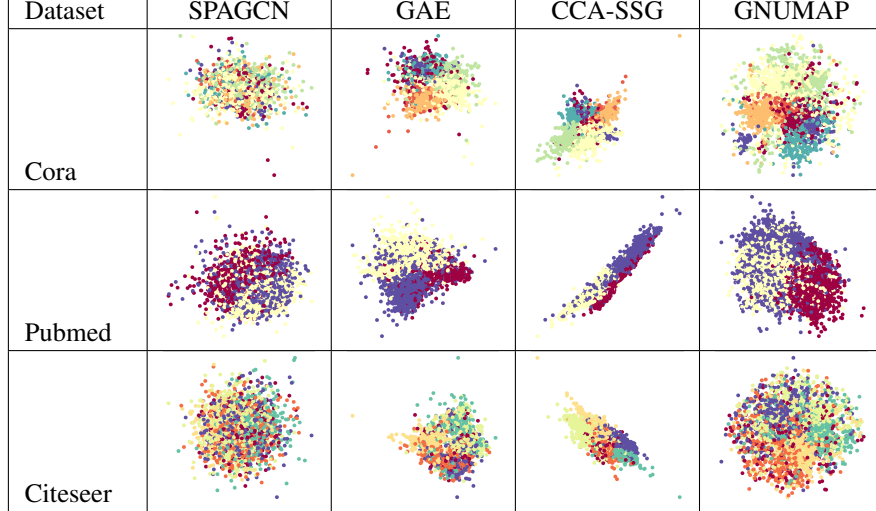


Figure 3: Node representation learning for real-world datasets Cora, Citeseer, Pubmed.

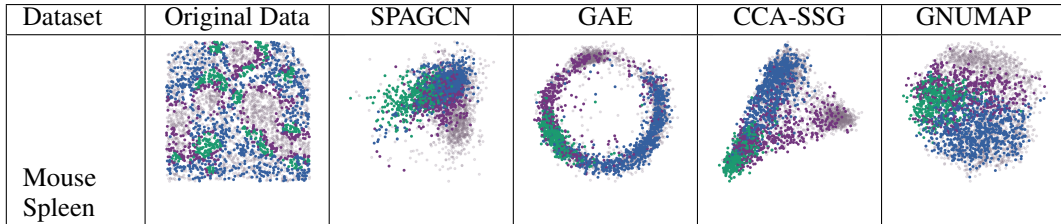


Figure 4. Node representation learning for Mouse Spleen dataset. Colours represent assigned ground truth cluster label. Blue denotes B-cells, purple denotes marginal zone B-cells, gray denotes non-B cells, and green denotes red pulp [28].

Table 2. Summary mean and standard deviation of proposed metrics over multiple experiments with real-world datasets Cora, Citeseer, Pubmed, and Mouse Spleen. The upward arrows next to the metric name denote a better performance with higher metrics, whereas the downward arrows denote a better performance with lower metrics. The best result is bolded, and the next best result is underlined.

Dataset	Model	Classification Accuracy \uparrow	Calinski Harabasz Score \uparrow	Davies Bouldin Score \downarrow
Cora	CCA-SSG	0.47 ± 0.11	107.12 ± 86.14	16.31 ± 25.76
	SPAGCN	0.31 ± 0.01	10.15 ± 4.25	17.24 ± 13.18
	GAE	0.50 ± 0.03	<u>104.19 ± 20.61</u>	<u>6.08 ± 6.18</u>
	GNUMAP	0.64 ± 0.04	87.90 ± 21.08	4.58 ± 3.19
Pubmed	CCA-SSG	0.59 ± 0.09	67.36 ± 69.68	14.66 ± 18.52
	SPAGCN	0.45 ± 0.03	16.99 ± 12.01	12.69 ± 14.60
	GAE	0.70 ± 0.01	144.36 ± 10.58	2.20 ± 0.17
	GNUMAP	0.67 ± 0.01	142.50 ± 19.38	2.81 ± 0.30
Citeseer	CCA-SSG	<u>0.50 ± 0.09</u>	159.64 ± 77.50	8.56 ± 17.91
	SPAGCN	0.26 ± 0.02	7.45 ± 3.52	23.18 ± 20.15
	GAE	0.47 ± 0.03	<u>81.11 ± 12.58</u>	5.78 ± 2.57
	GNUMAP	0.52 ± 0.03	51.81 ± 12.05	7.64 ± 4.38
Mouse Spleen	CCA-SSG	0.66 ± 0.02	138.08 ± 37.43	<u>2.30 ± 1.19</u>
	SPAGCN	0.60 ± 0.03	75.92 ± 40.20	4.72 ± 4.63
	GAE	<u>0.65 ± 0.02</u>	<u>126.91 ± 9.52</u>	2.11 ± 0.11
	GNUMAP	0.62 ± 0.02	79.78 ± 12.22	2.74 ± 0.32

this dataset. On the Mouse Spleen dataset, CCA-SSG and GAE perform best or second-best over all three evaluation metrics. GNUMAP is the third-best method across all metrics, and SpaGCN is the worst. However, since SpaGCN was designed specifically for biological application, such poor performance was unexpected, and this suggests the 5-nearest-neighboring-cells graph preprocessing method was unable to reflect the mouse spleen’s biological properties.

This allows for future exploration for a separate preprocessing pipeline for converting biological data to graph. We further emphasize again that for these examples, we chose the best performing hyperparameters for SPAGCN and CCA-SSG, thereby conferring these methods a significant advantage over the autoencoder setting.

5 Conclusion

With the exponential growth in data complexity, statisticians and computer scientists have recognized graphs as a modeling framework for high-dimensional data types. Therefore, modeling with graphs, predominantly through GNNs, is gaining traction in various areas, especially the biological [28, 1] domain. Through this work, we contribute to the ongoing research on unsupervised graph learning by proposing GNUMAP: a GNN inspired by theoretical research on the dimensionality reduction technique UMAP. Through our unique metrics that evaluate informativeness (classification accuracy), preservation of original graph information (agreement in local geometry, spearman correlation, frechet distance), and cluster quality (Davies-Bouldin score, Calinski-Harabasz score, silhouette score), we establish GNUMAP as a robust and expressive GNN embedding method that performs outperforms many existing GNN embedding methods, as well as dimensionality reduction methods depending on the task. Clear clustering of GNUMAP embeddings across synthetic geometric datasets as well as Cora, Citeseer, Pubmed, and Mouse Spleen further highlights the adaptive power of GNUMAP. GNUMAP performance can be characterized as “data-agnostic”—unlike state-of-the-art GNNs, there is minimal hyperparameter tuning required to enhance GNUMAP performance, allowing an easy application to any dataset.

Limitations and Future Work The reconstruction-based approach that we propose here in this paper, GNUMAP, is by design extremely simple, and its objective is interpretable. While it performs well on the examples that we provide here, this method is only valid for homophilic datasets – where edges encode similarities between nodes. However, this method also lends itself to natural extensions, such as accounting for cluster densities using the density coefficient of DenseMAP [25], to better capture the original data characteristics in low-dimensional embeddings.

References

- [1] Jian Hu, Xiangjie Li, Kyle Coleman, Amelia Schroeder, Nan Ma, David J Irwin, Edward B Lee, Russell T Shinohara, and Mingyao Li. Spagcn: Integrating gene expression, spatial location and histology to identify spatial domains and spatially variable genes by graph convolutional network. *Nature methods*, 18(11):1342–1351, 2021.
- [2] Franco Scarselli, Marco Gori, Ah Chung Tsoi, Markus Hagenbuchner, and Gabriele Monfardini. The graph neural network model. *IEEE Transactions on Neural Networks*, 20(1):61–80, 2009.
- [3] Thomas N. Kipf and Max Welling. Semi-supervised classification with graph convolutional networks, 2016.
- [4] Gabriele Partel and Carolina Wählby. Spage2vec: Unsupervised representation of localized spatial gene expression signatures. *The FEBS Journal*, 288(6):1859–1870, 2021.
- [5] Ruochi Zhang, Jianzhu Ma, and Jian Ma. Dango: Predicting higher-order genetic interactions. *bioRxiv*, pages 2020–11, 2020.
- [6] Junyi Li, Wei Jiang, Henry Han, Jing Liu, Bo Liu, and Yadong Wang. Scgslc: an unsupervised graph similarity learning framework for single-cell rna-seq data clustering. *Computational Biology and Chemistry*, 90:107415, 2021.
- [7] Satoshi Ishiai, Ikki Yasuda, Katsuhiro Endo, and Kenji Yasuoka. Graph-neural-network-based unsupervised learning of the temporal similarity of structural features observed in molecular dynamics simulations. *Journal of Chemical Theory and Computation*, 2024.
- [8] Hengrui Zhang, Qitian Wu, Junchi Yan, David Wipf, and Philip S. Yu. From canonical correlation analysis to self-supervised graph neural networks, 2021.
- [9] Petar Veličković et al. Deep graph infomax. *arXiv preprint arXiv:1809.10341*, 2018.
- [10] Shantanu Thakoor et al. Large-scale representation learning on graphs via bootstrapping. *arXiv preprint arXiv:2102.06514*, 2021.
- [11] Yanqiao Zhu et al. Deep graph contrastive representation learning. *arXiv preprint arXiv:2006.04131*, 2020.
- [12] Ilgee Hong, Huy Tran, and Claire Donnat. A simplified framework for contrastive learning for node representations. *arXiv preprint arXiv:2305.00623*, 2023.
- [13] Lan Huong Nguyen and Susan Holmes. Ten quick tips for effective dimensionality reduction. *PLoS computational biology*, 15(6):e1006907, 2019.

- [14] Ruizhi Xiang, Wencan Wang, Lei Yang, Shiyuan Wang, Chaohan Xu, and Xiaowen Chen. A comparison for dimensionality reduction methods of single-cell rna-seq data. *Frontiers in genetics*, 12:646936, 2021.
- [15] Ashley Babjac, Taylor Royalty, Andrew D Steen, and Scott J Emrich. A comparison of dimensionality reduction methods for large biological data. In *Proceedings of the 13th ACM International Conference on Bioinformatics, Computational Biology and Health Informatics*, pages 1–7, 2022.
- [16] Tamasha Malepathirana, Damith Senanayake, Rajith Vidanaarachchi, Vini Gautam, and Saman Halgamuge. Dimensionality reduction for visualizing high-dimensional biological data. *Biosystems*, 220:104749, 2022.
- [17] Leland McInnes, John Healy, and James Melville. Umap: Uniform manifold approximation and projection for dimension reduction, 2020.
- [18] Laurens van der Maaten and Geoffrey Hinton. Visualizing data using t-sne. *Journal of Machine Learning Research*, 9(86):2579–2605, 2008.
- [19] Leland McInnes, John Healy, Nathaniel Saul, and Lukas Grossberger. Umap: Uniform manifold approximation and projection. *The Journal of Open Source Software*, 3(29):861, 2018.
- [20] Junhai Zhai, Sufang Zhang, Junfen Chen, and Qiang He. Autoencoder and its various variants. In *2018 IEEE international conference on systems, man, and cybernetics (SMC)*, pages 415–419. IEEE, 2018.
- [21] Thomas N. Kipf and Max Welling. Variational graph auto-encoders, 2016.
- [22] Hengrui Zhang et al. From canonical correlation analysis to self-supervised graph neural networks. In *Advances in Neural Information Processing Systems*, volume 34, pages 76–89, 2021.
- [23] Joshua B. Tenenbaum, Vin de Silva, and John C. Langford. A global geometric framework for nonlinear dimensionality reduction. *Science*, 290(5500):2319–2323, 2000.
- [24] Mikhail Belkin and Partha Niyogi. Laplacian eigenmaps for dimensionality reduction and data representation. *Neural Computation*, 15(6):1373–1396, 2003.
- [25] Ashwin Narayan, Bonnie Berger, and Hyunghoon Cho. Density-preserving data visualization unveils dynamic patterns of single-cell transcriptomic variability. *bioRxiv*, 2020.
- [26] Zhilin Yang, William W. Cohen, and Ruslan Salakhutdinov. Revisiting semi-supervised learning with graph embeddings, 2016.
- [27] Yury Goltsev, Nikolay Samusik, Julia Kennedy-Darling, Salil Bhate, Matthew Hale, Gustavo Vazquez, Sarah Black, and Garry P Nolan. Deep profiling of mouse splenic architecture with codex multiplexed imaging. *Cell*, 174(4):968–981, 2018.
- [28] Zhenghao Chen, Ilya Soifer, Hugo Hilton, Leeat Keren, and Vladimir Jojic. Modeling multiplexed images with spatial-lda reveals novel tissue microenvironments. *Journal of Computational Biology*, 2020.
- [29] Asif Adil, Vijay Kumar, Arif Tasleem Jan, and Mohammed Asger. Single-cell transcriptomics: current methods and challenges in data acquisition and analysis. *Frontiers in Neuroscience*, 15:591122, 2021.
- [30] Martin Heusel, Hubert Ramsauer, Thomas Unterthiner, Bernhard Nessler, Günter Klambauer, and Sepp Hochreiter. Gans trained by a two time-scale update rule converge to a nash equilibrium. *CoRR*, abs/1706.08500, 2017.
- [31] David L. Davies and Donald W. Bouldin. A cluster separation measure. *IEEE Transactions on Pattern Analysis and Machine Intelligence*, PAMI-1(2):224–227, 1979.
- [32] T. Caliński and J Harabasz. A dendrite method for cluster analysis. *Communications in Statistics*, 3(1):1–27, 1974.
- [33] Peter J. Rousseeuw. Silhouettes: A graphical aid to the interpretation and validation of cluster analysis. *Journal of Computational and Applied Mathematics*, 20:53–65, 1987.

Appendix

A Metrics

Current approaches to evaluating embeddings generally fall into one of two types: (a) visual methods, where individuals visually inspect the learned embeddings to assess if they align with their expectations, and (b) classification-based methods. In the classification-based approach, it is presumed that there exists a set of labels, not used during training, which effectively represent the structure of the underlying data. In our work, we extend these latter metrics for application to manifold scenarios (which involve continuous structures rather than discrete ones) and quantify the performance of the learned representations using the following metrics.

General Metrics To assess the embedding quality, we propose measuring the agreement between the learned embedding space and the original data. This agreement can in particular be measured using:

- **Agreement in Local Geometry** We compute the percentage of overlap between the original graph’s k-nearest neighbors and knn graphs on the embedding space. A higher percentage denotes better local geometry preservation.

$$\frac{1}{n} \sum_{i=1}^n \frac{\# \text{ of overlapping neighborhood on } x_i}{\text{node degree}(x_i)}$$

- **Spearman Correlation** Inspired by a methodology introduced in [29], we evaluate the Spearman correlation between the pairwise distance in high-dimensional embedding space and embedding space from the model. Inspired by Isomap[23], the pairwise distance in the original space is evaluated by the shortest path distance, assuming that the geodesic distance on the manifold can be reasonably approximated by the shortest path distance. The pairwise distance in the low-dimensional space is evaluated by standard Euclidean distance. This metric evaluates the relationship between learned embedding space and the original graph using a monotonic function. The metric spans $[-1, 1]$ where -1 denotes a relationship modeled by a perfectly decreasing monotonic function, and vice versa. A higher Spearman correlation implies a similarity between the learned embedding and the original data.
- **Classification Accuracy** While our embeddings are unsupervised, we assume quality embeddings would form well-separated and helpful features for the support vector machine(SVM) multi-class classification problem. Consequently, we divide our manifold into different clusters (in intrinsic space) and assess the accuracy of the embedding space in recovering the different clusters through SVM with radial basis function(RBF) kernel. We record the average accuracy in predicting cluster labels from embedding space coordinates in a 10-fold. Higher accuracy thus implies the informativity of the learned embeddings.
- **Frechet Distance** Finally, we implemented the Frechet inception distance [30], a metric originally proposed to measure the similarity between images, to evaluate the 2d Frechet distance between the learned embedding coordinates and the original data. Smaller Frechet distance denotes better similarity between embedding and the original data coordinates.

Metrics for Clustered Data For data that are expected to form clusters (e.g. synthetic blobs, citation networks, Mouse Spleen gene expression prediction), we propose metrics evaluating the quality of cluster separation in the embedding space.

- **Davies Bouldin Score** This metric is the average ratio of inter-cluster distance to intra-cluster distance to the most similar cluster[31]. Davies Bouldin score is lower when clusters are concentrated and far apart. A lower score denotes better cluster separation, and the minimum score is zero.
- **Calinski Harabasz Score** This metric is the ratio of the sum of intra-cluster dispersion and of inter-cluster dispersion[32]. Calinski Harabasz score is higher when the intra-cluster variability is low and inter-cluster variability is high. A higher score indicates better score cluster separation.
- **Silhouette Score** This metric is the mean silhouette coefficient[33] of all data points. Let a be the mean intra-cluster distance and b be the mean nearest-cluster distance. Then, the silhouette coefficient for each data point is computed by $\frac{b-a}{\max(a,b)}$. Silhouette score is concerned with how similar a data point is to its assigned cluster compared to other clusters. The best value, 1, indicates well-separated and correctly assigned clusters, while the worst value, -1, often indicates that a sample is more similar to a different cluster. A silhouette score of 0 indicates overlapping clusters.

B Effect of α and β in Low Dimensional Representation

We will investigate the effect of α and β in eq-3. Recall the formula defining the edge connection probability in the low-dimensional space.

Table 3. Evaluated mean and standard deviation of proposed metrics for GNUMAP alterations for 100 synthetic swissroll experiments. The upward arrows next to metric names denote better performance with higher metrics, whereas the downward arrows denote better performance with lower metrics.

Note	a	b	Classification Accuracy \uparrow	Calinski Harabasz Score \uparrow	Davies Bouldin Score \downarrow	Spearman Correlation w/ Original Graph \uparrow	Overlap % of 50 Neighbours \uparrow
Baseline choice of $\alpha = \beta = 1$	1	1	0.28 ± 0.03	329.94 ± 82.75	2.44 ± 0.51	0.88 ± 0.07	0.96 ± 0.02
Smaller minimum distance	1.92	0.79	0.27 ± 0.02	373.00 ± 75.28	2.50 ± 0.69	0.93 ± 0.06	0.97 ± 0.02
Larger spread	0.13	0.81	0.28 ± 0.02	319.46 ± 84.10	2.56 ± 0.78	0.88 ± 0.07	0.96 ± 0.02
Larger spread, smaller minimum distance	0.15	0.79	0.28 ± 0.03	281.57 ± 97.08	2.70 ± 0.84	0.80 ± 0.16	0.95 ± 0.04
UMAP default	1.57	0.89	0.28 ± 0.03	314.90 ± 86.90	2.53 ± 0.50	0.88 ± 0.08	0.96 ± 0.02

$$q_{ij} = \frac{1}{1 + \alpha \times d(y_i, y_j)^{2\beta}}$$

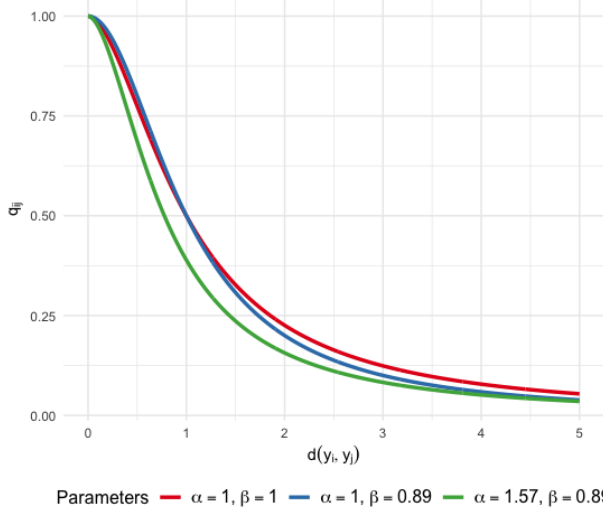


Figure 5: Comparisons of the effects of α and β on the probability q_{ij} according to eq-3

UMAP uses the family of curves $f(x) = \frac{1}{1 + \alpha x^{2\beta}}$ to compute the low-dimensional connection probability. If x , the distance between embeddings, is close to zero, connection probability becomes closer to 1. Else, the probability becomes closer to zero. UMAP’s low-dimensional connection probability calculation is dependent on α and β values. Figure 5 illustrates low-dimensional connection probability with respect to distance between embeddings for different α and β combinations.

C Effects of DBN

Decorrelation Batch Normalization (DBN).

DBN layer performs batch whitening, which removes linear correlation between input channels and, therefore, stabilizes GNN model convergence. DBN layer is effective in unrolling the higher-dimensional graph object into 2-dimensions, which can be confirmed both by visual inspection in Figure 6 and by metric evaluation in Table 4.

Table 4. Evaluated mean and standard deviation of proposed metrics for GNUMAP alterations for 100 synthetic Swissroll experiments. The upward arrows next to the metric name denote a better performance with higher metrics, whereas the downward arrows denote a better performance with lower metrics.

Architecture Choice	Calinski Harabasz Score \uparrow	Davies Bouldin Score \downarrow	Spearman Correlation w/ Original Graph \uparrow	Overlap % of 50 Neighbours \uparrow	Classification Accuracy \uparrow
Without DBN	305.39 ± 73.33	2.74 ± 0.76	0.87 ± 0.11	0.95 ± 0.03	0.26 ± 0.03
With DBN	314.90 ± 86.90	2.53 ± 0.50	0.88 ± 0.08	0.96 ± 0.02	0.28 ± 0.03

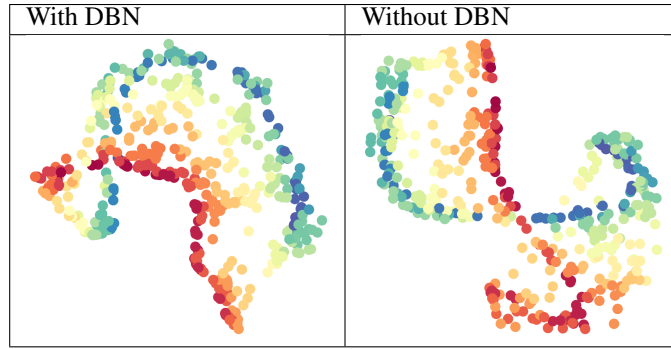


Figure 6: GNUMAP synthetic Swissroll embeddings with and without DBN layer.

D Additional Figures

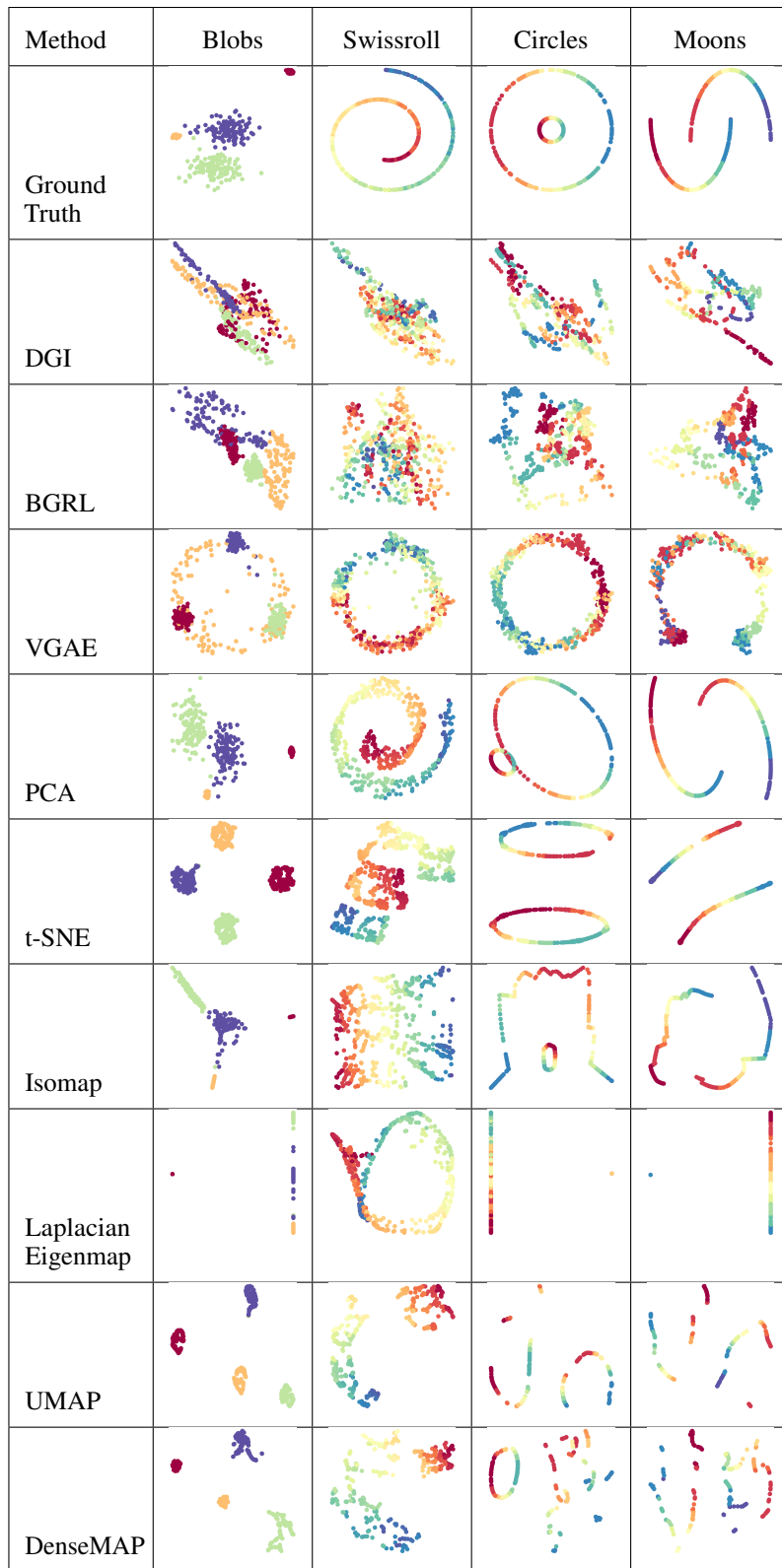


Figure 7. Node representation learning for 4 synthetic datasets: Blobs, Swissroll, Circles, and Moons. Each image represents a different method of visualization.